Renewable Sources and Energy Storage Optimization to Minimize the Global Costs of Railways

Nakaret Kano, *Student Member, IEEE*, Zhongbei Tian, Nutthaka Chinomi, Xiaoguang Wei and Stuart Hillmansen

Abstract—**Climate change is one of the biggest global issues for humanity these days, and its effect has become more severe. The transport sector accounts for around 30% of greenhouse gas emissions, which need to be decarbonized urgently. Railway electrification is one of the low-carbon solutions, but it still relies on power grids causing carbon emissions. To further decarbonize electric railways, the renewable energy sources (RESs) and energy storage system (ESS) integration scheme for railway traction power network has been proposed. This paper developed the energy management system to calculate the energy flow and global cost. Moreover, contact wire loss and conversion loss were considered. The optimization problem to find the optimal capacity and location of the PV farm, wind farm and energy storage system to achieve the lowest global daily costs was solved by the Brute Force Algorithm. The traction network of the High Speed 2 Railway in the UK has been taken as a case study. Results revealed that the global cost and carbon emissions are reduced considerably with both ESS and RESs installed. In the scenario of the ESS alone, 1.3% of the global cost is saved by capturing the regenerative energy and reusing it. Furthermore, this figure goes up to 10% and 62% when the PV and wind farms are integrated, respectively. When considering all variables, it is found that installing the wind farm is a more economical option than the PV farm. The study also shows that the optimal locations to install the plants and ESS vary by scenario.**

Index Terms— **Traction power system, renewable energy source (RES), regenerative braking energy, energy storage system (ESS), optimal sizing.**

I. INTRODUCTION

With the global trend to reduce carbon emissions, the UK government had set a goal to reach net-zero emissions by 2050 [1]. All industrial sectors, including the railway sector are seeking ways to achieve this goal. Transitioning from the reliance on fossil fuels is one of the most effective ways to reduce emissions. For an electrified railway system, carbon emissions are dependent on the source of electricity, which is supplied by the national grid. A lot of research contributes to carbon reduction with the integration of renewable energy sources (RES) into the railway power system and the utilization of energy storage systems (ESS) and regenerative braking energy (RBE).

Many research articles provided a study of the RES integration and ESS utilization for the AC railway systems. The advantages and disadvantages of various RES integration schemes for AC railway systems are discussed in [2] and [3]. Although RES integration to the medium voltage DC railway microgrid is more suitable, the potential to improve the energy performance for the AC railway microgrid cannot be neglected. Sida T. [4] presented a hybrid energy storage system (HESS) for a high-speed railway traction substation, which includes the supercapacitor and vanadium redox battery to capture the RBE. An improved mutation-based particle swarm optimization is introduced to obtain the optimal size of HESS with a minimum net present value. Wenli D. [5] proposed a hybrid traction substation with PV integration without altering the architecture. Boudoudouh et al. [6] proposed a distributed energy management for a railway microgrid with a hybrid substation, which includes a PV plant, wind farm, and ESS. The design can reduce the subscribed power and eliminate the voltage drop/rise along the line.

Energy management system (EMS) for railway systems has been widely researched to optimize energy consumption. Novak et al. [7] presented a railway EMS using hierarchical coordination of several trains' energy consumption and traction substation. Razik et al. [8] presented a prototype implementation of a railway EMS, which is a distributed system coordinating rolling stock, substations, and wayside resources. The overall energy demand, power consumption, and cost optimization can be performed in both offline and real-time processes. Tian et al. [9] proposed an integrated optimization method to solve the energy-saving problems of a multi-train traction power network, with consideration of train movement and electrical power flow. An electric railway smart microgrid system, with multiple RES and ESS integrated via a railway power conditioner (RPC), is proposed by Chen [10], to reduce railway energy consumption and improve the power quality. A

Nakaret Kano is with the University of Birmingham, Birmingham, UK, B15 2TT (e-mail: nxk887@student.bham.ac.uk).

Zhongbei Tian is with the Department of Electrical Engineering and Electronics, University of Liverpool, Liverpool, UK, L69 3GJ (e-mail: zhongbei.tian@liverpool.ac.uk).

Nutthaka Chinomi is with the University of Liverpool, Liverpool, UK, L69 3GJ (e-mail: n.chinomi@liverpool.ac.uk).

Xiaoguang Wei is with the School of Electrical Engineering, Southwest Jiaotong University, Chengdu 610031, China (e-mail: wei_xiaoguang@126.com).

Stuart Hillmansen is with the Department of Electronic, Electrical and Systems Engineering, University of Birmingham, Birmingham, UK, B15 2TT (e-mail: s.hillmansen@bham.ac.uk).

power-to-gas (P2G) technology is introduced to absorb the excess energy from RES and RBE.

Several research articles studied the EMS considering the energy and cost evaluation. Yichen Y. [11] proposed a flexible smart traction power supply system (TPSS) with the utilization of an AC-DC-AC traction substation to solve the power quality issues, the low utilization rate of RBE, and the inability to use the distributed generation along the railway. The optimal operation cost can be reduced up to 42.17% compared with the traditional TPSS. D'Arco et al. [12] proposed PV integration schemes for AC railways and analyzed the cost and power losses. The study revealed that the PV farm power rating is the critical factor that determined the cost of the system. Liu et al. [13] proposed an EMS of a co-phase traction substation with PV and HESS, to minimize the operation cost. The results achieved a cost saving of 4.99%. Aguado et al. [14] proposed a railway model including PV, wind, RBE and HESS, to optimize the total operation cost. With RES and ESS, there is an improvement of 33.22% and 9.63% in costs and energy savings, respectively. Salkuti [15] proposed an optimal railway operation by balancing the energy flow between the grid, traction and braking trains, RES, and ESS, to minimize the total operation cost. The optimization results, solved by using GAMS/CONOPT, are verified with a differential evolution algorithm. Park et al. [16] proposed an AC railway model with the integration of RES and HESS and the utilization of RBE to optimize the total operation cost. The proposed non-linear programming problem was solved by a differential evolution algorithm and achieved a total cost savings of 13.05%. Şengör et al. [17] suggested a mixed integer linear programming model of a railway station with ESS and PV integration. The impact of RBE and different pricing schemes are evaluated. The authors aimed to minimize the total daily cost of the station's electricity consumption as well as to evaluate the RBE, and ESS. The combination of PV, ESS and RBE reduces the cost by around 30% compared to the base case. Chen et al. [18] proposed a flexible TPSS with HESS and PV to improve the power quality and eliminate the neutral zone. A sparrow search algorithm is used to optimize for the lowest cost which includes the investment, the replacement, the operation and maintenance (O&M), and the electricity costs. The model could achieve a 13.55% cost reduction.

The integration of RES and ESS along with the utilization of RBE could improve the operational cost and reduce energy consumption, which can be proven by the various models of the research presented. However, most of these research articles have studied the integration of RES at the traction substation and the size of RES is greatly affected by the limited space. Nevertheless, by integrating the RES along the railway, the issue of the limited RES size could be alleviated. In addition, the aspect of contact wire loss was not considered in the above literature. Therefore, this study proposed the integration of distributed RES and ESS into the railway overhead line via a static frequency converter (SFC). The proposed model of the railway system includes the analysis of the contact wire loss. Moreover, the location and capacity of PV farms, wind farms,

and ESS are optimized to obtain minimum global daily cost, which includes operation and investment costs. The main contributions of this study are:

1. A renewable energy sources and energy storage system integration scheme is proposed for retrofitting the conventional high-speed railway power system without modifying the architecture.

2. A comprehensive model with an energy management system is developed to calculate energy consumption and cost considering the operation and the investment, including the railway network contact wire loss.

3. Brute force method is used to optimize the sizing and location of the RES and ESS and minimize the global daily cost, which is verified in a case study.

The paper is organized as follows. The proposed scheme and the modeling method are illustrated in Section 2. The details of the energy management system and the cost optimization are presented in Sections 3-4. The proposed method is verified with a case study in Section 5. Finally, the conclusion is given in Section 6.

II. RENEWABLE RAILWAY MODELING METHOD

The proposed RES and ESS integration scheme into an AC railway power supply system is presented in Fig. 1. The AC railway is separated into multiple feeding sections by neutral sections. D_{ess1} and D_{ess2} are the installed ESS locations for the left and right feeding sections (km), respectively.
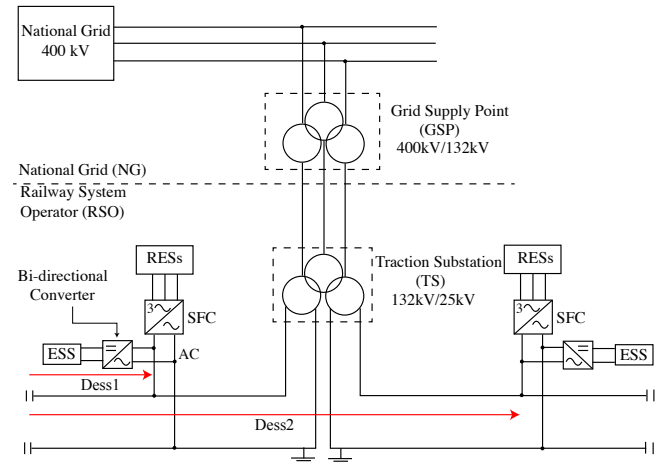

Fig. 1. Integration scheme of RES and ESS into AC railway power supply system.

A. Train Movement Modeling

The movement of a train along the railway track follows Newton's law of motion as shown in (1). For a train to move, the traction effort must overcome the resistive forces, which comprise the gradient force, the train motion resistance, and the curvature resistance [9].

$$M \cdot (1 + \lambda) \cdot a = F - M \cdot g \cdot sin(\alpha) - F_D - F_C \qquad (1)$$

where M is the train mass (kg), λ is the rotary allowance, a is the train acceleration (m/s^2), F is the tractive effort (N), g is the gravity acceleration (m/s^2), α is the angle of gradient (rad), F_D is

the Davis' equation of motion resistance (N), and F_C is the curve resistance (N).

The train mechanical power at wheel can be computed by equation (2) as shown below:

$$P_{tr,mech}^t = F^t \cdot v^t \qquad (2)$$

where $P_{tr,mech}^t$ is the train mechanical power at wheel at time t (W), F^t is the tractive force at time t (N) and v^t is the train velocity at time t (m/s).

For an electric train equipped with a regenerative brake, the traction and regenerative power are calculated using (3) and (4), respectively. The net electrical power is given by (5).

$$P_{traction}^t = \frac{P_{traction,mech}^t}{\eta_{motor}} \qquad (3)$$

$$P_{regen}^t = P_{regen,mech}^t \cdot \eta_{motor} \qquad (4)$$

$$P_{tr}^t = P_{traction}^t + P_{regen}^t \qquad (5)$$

where η_{motor} is the efficiency of motor (p.u.), which is set to 0.9, $P_{traction,mech}^t$ and $P_{traction}^t$ is the mechanical and electrical tractive power (W), $P_{regen,mech}^t$ and P_{regen}^t is the mechanical and electrical regenerative braking power (W) and P_{tr}^t is the net electrical power of trains (W).

A train power profile is created considering neutral sections. Fig. 2 illustrates a single train profile with one traction substation and two feeding sections. To obtain the multiple train profile for an entire day, all train profiles in the same feeding section are combined into one single profile. Note that all trains are identical in terms of rolling stock specification, driving style and route.
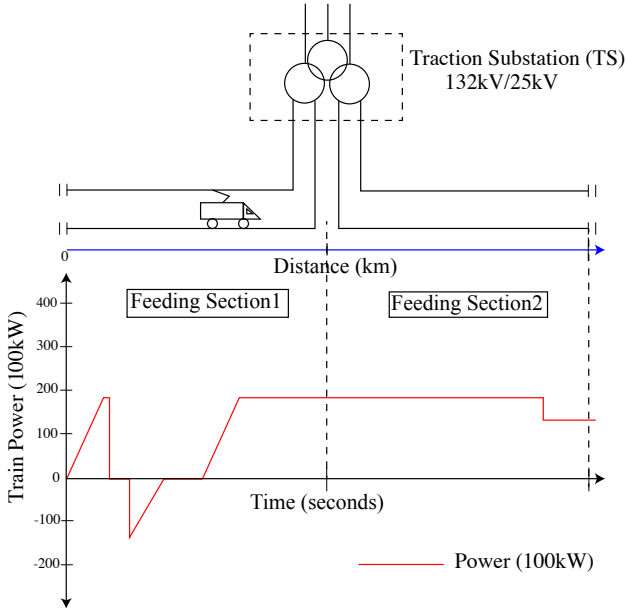

Fig. 2. Single train power profile in two feeding sections.

B. RES Modelling

PV and wind farms are connected to an SFC via a three-phase 690V/33kV transformer, which is then integrated into the 25 kV railway power supply system, as shown in Fig. 3.
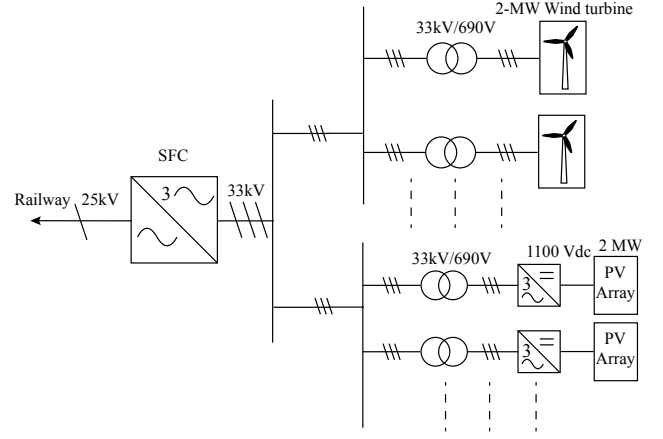

Fig. 3. A single-line diagram of solar PV farm and wind farm connected to railway overhead line via SFC.

1) Solar PV model

A large-scale PV farm is formulated of several 2 MW PV arrays. The electrical power generated by a PV farm is given in (6) [19].

$$P_{pv}^t = s^t \cdot A \qquad (6)$$

where P_{pv}^t is the power produced by the PV farm at time t (W), s^t is the solar irradiance at time t (W/m²) and A is the surface area of the PV farm (m²).

2) Wind turbine model

A large-scale wind farm is formulated of several 2 MW wind turbines. The electrical power generated by a wind turbine is given in (7) [20]–[22].

$$P_{wind}^t = \begin{cases} 0 & , & v_w^t < v_{ci} \\ P_{wind}^{rated} \cdot \frac{(v_w^t)^a - v_{ci}^a}{v_r^a - v_{ci}^a}, & v_{ci} \le v_w^t \le v_r \\ P_{wind}^{rated} & , & v_r < v_w^t < v_{co} \\ 0 & , & v_w^t > v_{co} \end{cases} \qquad (7)$$

where v_w^t is the wind speed at time t (m/s), P_{wind}^t is the power output of the wind farm at time t (W), P_{wind}^{rated} is the rated generation capacity of the wind farm (W), v_{ci} is the cut-in wind speed (m/s), v_{co} is the cut-out wind speed (m/s), v_r is the rated wind speed (m/s), and a is the Weibull shape parameter.

C. Conversion Device Modeling

1) Power inverter

For a grid-connected PV farm, an inverter is necessary to convert DC to AC power. Equation (8) is utilized to simulate the efficiency [23]. For ESS, a bi-directional converter, which acts as a rectifier during the charging process and an inverter during the discharging process, is required [24]. The efficiency of the bi-directional converter can be calculated using (9). Equation (10) shows that the rated power of the converter is equivalent to the rated power of the energy storage.

$$\eta_{inv,pv}(P_{dc,pu}) = A_{inv,pv} + B_{Inv,pv} \cdot P_{dc,pu} + \frac{C_{inv,pv}}{P_{dc,pu}} \qquad (8)$$

$$\eta_{conv,ess}(P_{ess,pu}) = A_{conv,ess} + B_{conv,ess} \cdot P_{ess,pu} + \frac{C_{conv,ess}}{P_{ess,pu}} \qquad (9)$$

$$S_{conv,ess} = P_{ess}^{rated} \qquad (10)$$

where $\eta_{inv,pv}$ and $\eta_{conv,ess}$ are the PV inverter efficiency and the bi-directional converter efficiency (%), $P_{dc,pu}$ is ratio of the DC input power and the inverter rated power (p.u.), $P_{ess,pu}$ is the ratio of the ESS input power and the converter rated power (p.u.). $A_{inv,pv}$, $B_{inv,pv}$, $C_{inv,pv}$, $A_{conv,ess}$, $B_{conv,ess}$ and $C_{conv,ess}$ are the parameters determined using information and the method in [23],[25]. It should be noted that the three parameters for the bi-directional converter are given the same values as the PV inverter.

2) Transformer

Transformers are not ideal due to copper and core losses. The transformer efficiency is given by (11) [26].

$$\eta_{tf}(k) = \frac{k \cdot S_{tf}}{k \cdot S_{tf} + k^2 \cdot P_k + P_0} \tag{11}$$

where $\eta_{tf}(k)$ is the transformer efficiency at load factor k (p.u.), S_{tf} is the transformer rated power based on P_k (VA), P_0 is the core loss at the rated voltage and frequency (W), and P_k is the load loss at the rated current and frequency (W).

3) Static frequency converter

SFC is utilized to convert a three-phase to a single-phase power without changing the frequency [27]. In this study, the three-phase output powers from the PV and wind farms are converted to DC voltages via a DC link and then inverted to single-phase AC powers. The rated capacity of an SFC is a sum of PV and wind farm capacity, as presented in (12). Assuming that the efficiency curve of the SFC has the same characteristic as the PV inverter efficiency curve, (13) is derived from (8).

$$S_{sfc} = P_{pv}^{rated} + P_{wind}^{rated} \tag{12}$$

$$\eta_{sfc}(P_{3p-AC,pu}) = A_{sfc} + B_{sfc} \cdot P_{3p-AC,pu} + \frac{C_{sfc}}{P_{3p-AC,pu}} \tag{13}$$

where S_{sfc} is the SFC rated capacity (MVA), η_{sfc} is the static frequency converter efficiency (%), $P_{3p-AC,pu}$ is a ratio of the three-phase AC input powers of SFC and S_{sfc} (p.u.), A_{sfc}, B_{sfc}, and C_{sfc} are assumed the same values as the PV inverter.

Based on an assumption that they are modular systems, the number of units can be customized to obtain the required power rating. For instance, a 10 MW energy storage will require 5 units of bi-directional converters. All parameters for the conversion devices are displayed in TABLE I.

TABLE I
PARAMETERS FOR THE CONVERSION DEVICES

Inverters and SFC per unit		Transformers for PV and Wind farms	
Capacity (MVA)	2	S_{tf} (MVA)	2.1
$A_{inv,pv}, A_{conv,ess}, A_{sfc}$	99.34	Voltage (V)	690/33000
$B_{inv,pv}, B_{conv,ess}, B_{sfc}$	-1.472	P_o (kW)	2.1
$C_{inv,pv}, C_{conv,ess}, C_{sfc}$	-0.1694	P_k (kW)	24.34

III. ENERGY MANAGEMENT SYSTEM

A. Operation Strategies of Energy Storage System (ESS)

ESS is utilized to absorb excess energy from RES and residual RBE. The flowchart of the 19 ESS working modes is illustrated in Fig. 4. Several parameters define the ESS working modes, i.e., the train driving modes, the RES size, the State of Charge (SOC), and the ESS power.

The ESS working modes are grouped in three states, as presented in TABLE II and the stored energy for each state is calculated by (14). In *idle state*, the ESS has no operation, and the energy level does not change, for instance, when trains require no power or are in coasting mode. In *charging state*, the ESS charges and the energy level increases. In *discharging state*, the energy level decreases as it releases energy to supply loads.
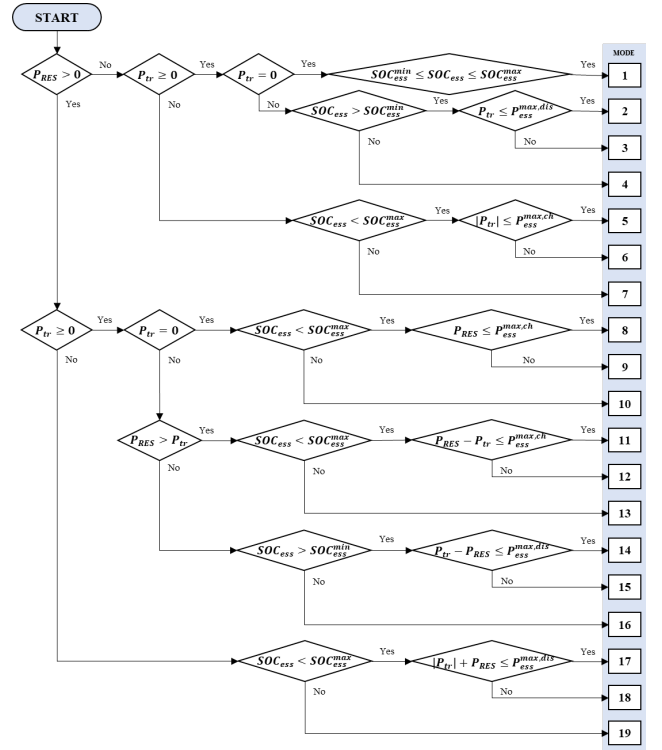

Fig. 4. The flowchart of the ESS control strategy.

TABLE II
POWER FOR EACH MODE OF THE ESS

State	Mode	Power
Idle	1, 4, 7, 10, 13, 16, 19	$P_{ess}^{ch,t} = P_{ess}^{dis,t} = 0$
Charging	6, 9, 12, 18	$P_{ess}^{ch,t} = P_{ess}^{max,ch}$
	5	$P_{ess}^{ch,t} = P_{tr}^t$
	8	$P_{ess}^{ch,t} = P_{res}^t$
	11	$P_{ess}^{ch,t} = P_{res}^t - P_{tr}^t$
	17	$P_{ess}^{ch,t} = P_{res}^t + |P_{tr}^t|$
Discharging	3, 15	$P_{ess}^{dis,t} = P_{ess}^{max,dis}$
	2	$P_{ess}^{dis,t} = P_{tr}^t$
	14	$P_{ess}^{dis,t} = (P_{tr}^t - P_{res}^t)$

$$E_{ess}^{t+1} = \begin{cases} E_{ess}^t + \dfrac{P_{ess}^{ch,t} \cdot \eta_{ess}^{ch} \cdot \Delta t}{3600}, & \text{charging} \\ E_{ess}^t, & \text{idle} \\ E_{ess}^t - \dfrac{P_{ess}^{dis,t} \cdot \Delta t}{3600 \cdot \eta_{ess}^{dis}}, & \text{discharging} \end{cases} \quad (14)$$

Furthermore, when the last train of the day finishes its operation, the ESS is controlled to discharge the stored energy at rated power to the grid until it reaches the lower limit of SOC to prepare to absorb excess power from the next day. Equation (15) denotes the SOC of the ESS. The limits of charging and discharging power are shown in (16) and (17). Additionally, it is assumed that the upper limits are identical to the rated power capacity as shown in (18). Equations (19) and (20) indicated that the SOC and the stored energy should be in a suitable range to prevent over-charge and over-discharge.

$$SOC_{ess}^t = \frac{E_{ess}^t}{E_{ess}^{rated}} \cdot 100 \quad (15)$$

$$0 \leq P_{ess}^{ch,t} \leq P_{ess}^{max,ch} \quad (16)$$

$$0 \leq P_{ess}^{dis,t} \leq P_{ess}^{max,dis} \quad (17)$$

$$P_{ess}^{max,ch} = P_{ess}^{max,dis} = P_{ess}^{rated} \quad (18)$$

$$SOC_{ess}^{min} \leq SOC_{ess}^t \leq SOC_{ess}^{max} \quad (19)$$

$$SOC_{ess}^{min} \cdot E_{ess}^{rated} \leq E_{ess}^t \leq SOC_{ess}^{max} \cdot E_{ess}^{rated} \quad (20)$$

where $P_{ess}^{ch,t}$, $P_{ess}^{dis,t}$, $P_{ess}^{max,ch}$ and $P_{ess}^{max,dis}$ are the charging power at time t (W), the discharging power at time t (W), the maximum charging power (W) and the maximum discharging power (W), respectively. P_{ess}^{rated} is the rated power capacity of the energy storage (W), P_{res}^t is the total power from RES (W), P_{tr}^t is the net power of trains in the feeding section at time t (W), E_{ess}^t and E_{ess}^{t+1} are the stored energy in the ESS at time t and $t + 1$ (Wh), η_{ess}^{ch} and η_{ess}^{dis} are the charge and discharge efficiency (p.u.), E_{ess}^{rated} is the rated energy capacity of the ESS (Wh), SOC_{ess}^t is the state of charge at time t (%), SOC_{ess}^{min} and SOC_{ess}^{max} are the lower and upper limits of SOC (%), Δt is the time interval which is set to 20 (s).

B. Energy Evaluation

1) Contact wire loss calculation

The contact wire loss is dependent on two main factors; the magnitude of the conductor resistance and the current flows from/to trains. With RES and ESS, the current flows depend on the ESS working modes, and the integrating location affects the contact wire losses, as denoted in (21). The total energy loss in the contact wire is given in (22).
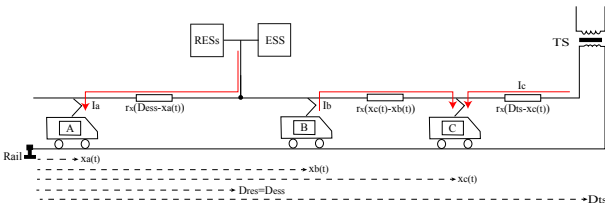

Fig. 5. Current flows with multiple trains in a feeding section.

$$P_{CWloss}^t = I_a^{t\,2} \cdot r \cdot (D_{ess} - x_a^t) + I_b^{t\,2} \cdot r \cdot (x_c^t - x_b^t) + I_c^{t\,2} \cdot r \cdot (D_{ts} - x_c^t) \quad (21)$$

$$E_{CWloss} = \sum_{t=1}^{N} P_{CWloss}^t \cdot \Delta t/3600 \quad (22)$$

where P_{CWloss}^t is the electrical loss on the contact wire (W), I_a^t is the current required by traction train A (A), I_b^t is the current supplied from braking train B to traction train C (A), I_c^t is the current supplied to train C by the grid (A), x_a^t is the location of train A (km), x_b^t is the location of train B (km), x_c^t is the location of train C at time t (km), D_{ess} is the location of the ESS and RES (km), D_{ts} is the location of traction substation (km), r is the electrical resistance of contact wire per unit length (Ω/km) and E_{CWloss} is the energy loss in contact wire (Wh).

2) Train energy consumption

The electrical traction energy and the RBE can be calculated using (23) and (24), respectively.

$$E_{traction} = \sum_{t=1}^{N} P_{traction}^t \cdot \Delta t/3600 \quad (23)$$

$$E_{regen} = \sum_{t=1}^{N} P_{regen}^t \cdot \Delta t/3600 \quad (24)$$

where $E_{traction}$ is the energy required by traction trains (Wh) and E_{regen} is the RBE from time index $t = 1$ to N (Wh).

3) Solar PV energy

The generated electrical energy of a solar PV is computed by (25), where E_{pv} is the energy of the PV farm during time index $t = 1$ to N (Wh).

$$E_{pv} = \sum_{t=1}^{N} P_{pv}^t \cdot \Delta t/3600 \quad (25)$$

4) Wind energy

The energy from the wind turbine is calculated by (26), where E_{wind} is the energy from a wind farm during time index $t = 1$ to N (Wh).

$$E_{wind} = \sum_{t=1}^{N} P_{wind}^t \cdot \Delta t/3600 \quad (26)$$

IV. GLOBAL COST OPTIMIZATION

The main goal of the optimization is to find the best location and size for the RES and ESS. Therefore, the global cost, which is the sum of the daily operation and investment cost, becomes the minimum. The details of the objective function and constraints are mentioned below:

A. Objective Function

Minimize:

$$C_{total} = C_{buy} + C_{ess} + C_{sfc} + C_{pv} + C_{wind} + C_{carbon} - C_{sell} \quad (27)$$

where C_{total} is the global cost, C_{buy} is the total cost of purchasing power from the grid, C_{ess} is the total cost of ESS, C_{sfc} is the cost of the SFC, C_{pv} is the cost of PV farm, C_{wind} is the cost of the wind farm, C_{carbon} is the carbon emissions cost and C_{sell} is the total revenue from selling power back to the

grid. All costs are based on £/day.

Equation (28) presents the total daily cost of purchasing power from the grid. The total cost of ESS is a sum of the capital cost and the O&M cost, which can be calculated using (29). It can be seen from (30) that there are two parts of ESS capital cost; one is the cost of energy capacity (£/MWh) which is dependent on the amount of energy that can be stored, and the other is the cost of power capacity (£/MW) which is dependent on the maximum rate at which the system can transfer or discharge electricity [28]. Equation (31) is used to calculate the ESS storage time t_{ess} (hr), which refers to the time spent to discharge the energy storage from full to empty or vice versa. The O&M cost is assumed to be 10% of the ESS capacity cost per year. Hence, for the entire operation lifetime, the O&M cost can be computed using (32). The SFC cost is shown in (33).

$$C_{buy} = \sum_{t=1}^{N} \frac{P_{buy}^t \cdot \Delta t \cdot c_{buy}}{3600 \cdot 10^6} \qquad (28)$$

$$C_{ess} = \left(C_{ess}^{cap} + C_{ess}^{om}\right) \cdot \frac{1}{365 \cdot T_{ess}} \qquad (29)$$

$$C_{ess}^{cap} = \left(c_{ess,MWh} + \frac{c_{ess,MW}}{t_{ess}}\right) \cdot \frac{E_{ess}^{rated}}{10^6} \qquad (30)$$

$$t_{ess} = \frac{E_{ess}^{rated}}{P_{ess}^{rated}} \qquad (31)$$

$$C_{ess}^{om} = 0.1 \cdot c_{ess,MW} \cdot P_{ess}^{rated} \cdot T_{ess} \qquad (32)$$

$$C_{sfc} = \frac{S_{sfc} \cdot c_{sfc}}{365 \cdot 10^6 \cdot u_{sfc} \cdot T_{sfc}} \qquad (33)$$

Solar PV farm and wind farm costs are presented in (34) and (35). There are three main costs considered, i.e., the pre-development cost, the construction and infrastructure cost, and the O&M cost [29]. Furthermore, as power from the grid is not wholly generated from clean energy sources, the carbon cost is considered, as seen in (36). The carbon emission is estimated using average carbon intensity (CI, gCO2/kWh).

$$C_{pv} = \frac{P_{pv}^{rated}\left(c_{pd,pv} + c_{con,pv} + c_{om,pv} \cdot T_{pv}\right)}{365 \cdot T_{pv}} \qquad (34)$$

$$C_{wind} = \frac{P_{wind}^{rated}\left(c_{pd,wind} + c_{con,wind} + c_{om,wind} \cdot T_{wind}\right)}{365 \cdot T_{wind}} \qquad (35)$$

$$C_{carbon} = \sum_{t=1}^{N} \frac{P_{buy}^t \cdot \Delta t \cdot CI \cdot c_{carbon}}{3600 \cdot 10^6} \qquad (36)$$

Finally, due to the intermittency of renewable generation, there is a mismatch between demand and supply resulting in excess energy, which is sold to the grid at a lower rate than the purchasing price. Equation (37) shows the revenue from selling the excess energy.

$$C_{sell} = \sum_{t=1}^{N} \frac{P_{sell}^t \cdot \Delta t \cdot c_{sell}}{3600 \cdot 10^6} \qquad (37)$$

where c_{buy} is the cost per MWh of buying energy from the grid, c_{sell} is the cost per MWh of selling power to the grid, C_{ess}^{cap} and C_{ess}^{om} are the capital cost and the operation and maintenance cost of energy storage, $c_{ess,MW}$ is the cost per MW of ESS power capacity, $c_{ess,MWh}$ is the cost per MWh of ESS energy capacity, c_{sfc} and u_{sfc} are the cost and capacity per unit of SFC, c_{pd},

c_{con} and c_{om} are the pre-development cost, the construction and infrastructure cost and the O&M cost per MW of PV and wind, T_{ess}, T_{sfc}, T_{pv} and T_{wind} are the operational lifetime of the ESS, SFC PV and wind respectively, P_{buy}^t is the power purchased from the grid at time t, P_{sell}^t is the excess power sold to the grid at time t, N is the total number of time intervals in a day (4320).

It should be noted that C_{ess}, C_{sfc}, C_{pv} and C_{wind} are scaled down to one-day time horizon to match C_{buy}, C_{sell} and C_{carbon} and reduce the computational burden.

B. Variables

There are five variables to be optimized as follows:
1. *Location of the energy storage system and renewable energy sources (D_{ess}, km)*: This variable indicates the integrating location of the ESS, PV and wind farm.
2. *Rated energy capacity of the energy storage (E_{ess}^{rated}, Wh)*: This variable indicates how much energy can be stored from empty until fully charged.
3. *Rated power capacity of the energy storage (P_{ess}^{rated}, W)*: This variable indicates how much power can flow in and out of the energy storage in any given instant.
4. *Rated power of the PV farm (P_{pv}^{rated}, W)*: This variable presents the maximum power produced by the PV farm.
5. *Rated power of the wind farm (P_{wind}^{rated}, W)*: This variable presents the maximum power produced by the wind farm.

C. Constraints

1) Constraints of the ESS

Equations (16) to (20) present the constraints of the ESS. In addition, (38) and (39) present the upper limits of the energy and power capacity. Moreover, to ensure that the energy storage can supply the train during travelling in the section in case of a power outage, equation (40) is applied.

$$0 \leq E_{ess}^{rated} \leq E_{ess}^{limit} \qquad (38)$$

$$0 \leq P_{ess}^{rated} \leq P_{ess}^{limit} \qquad (39)$$

$$t_{ess} \geq T_{tr,fs} \qquad (40)$$

where E_{ess}^{limit} and P_{ess}^{limit} are the maximum rated energy capacity (Wh) and power capacity of the ESS (W), respectively, $T_{tr,fs}$ is the duration of a train traveling in the feeding section (hr).

2) Constraints of solar PV and wind farms

Equation (41) indicates that power generated from solar PV must not exceed the rated capacity which is limited by (42). Similarly, (43) and (44) are constraints of the wind farm.

$$0 \leq P_{pv}^t \leq P_{pv}^{rated} \qquad (41)$$

$$0 \leq P_{pv}^{rated} \leq P_{pv}^{limit} \qquad (42)$$

$$0 \leq P_{wind}^t \leq P_{wind}^{rated} \qquad (43)$$

$$0 \leq P_{wind}^{rated} \leq P_{wind}^{limit} \qquad (44)$$

where P_{pv}^{rated} and P_{wind}^{rated} are the rated capacity of PV and wind farms (W), P_{pv}^{limit} and P_{wind}^{limit} is the upper limit of the PV farm and wind farm capacity (W).

3) Constraints of the contact wire

To prevent the contact wire from overloading, the maximum current carrying capacity is set. Therefore, the capacity of PV and wind farms must be less than this limit, as shown in (45), where P_{cw}^{rated} is the maximum capacity of the contact wire (W).

$$P_{pv}^{rated} + P_{wind}^{rated} \leq P_{cw}^{rated} \tag{45}$$

The current carrying capacity of the conductor used in contact wire in this study is 1594 A with a wind velocity of 1 m/s, conductor temperature of 80 degrees Celsius at an ambient temperature of 20 degrees Celsius [30]. The type of conductor is 626-AL1. Therefore, with a working voltage of 25 kV, this conductor can carry approximately 40 MW of power.

4) Power balance

Equation (46) describes the power balance of the demand and supply. Any excess power is sold to the grid. On the other hand, power is required from the grid in case of insufficiency.

$$P_{traction}^t + P_{cwloss}^t + P_{conv}^t + P_{ess}^{ch,t} + P_{sell}^t$$
$$= P_{buy}^t + P_{pv}^t + P_{wind}^t + P_{ess}^{dis,t} + P_{regen}^t \tag{46}$$

where P_{conv}^t is power losses in the conversion devices i.e., inverter, transformer and the SFC (W).

V. CASE STUDY

A. Description

The route and overhead line information from the first phase of the HS2 project in the UK is used. The feeding sections are divided into six sections for the entire route from London to Birmingham, as illustrated in Fig. 6. The route and infrastructure information are presented in TABLE III and TABLE IV. Nevertheless, only the first two feeding sections with a total length of 48 km are considered in the case study. The same methodology can be applied to obtain optimization results for other feeding sections.
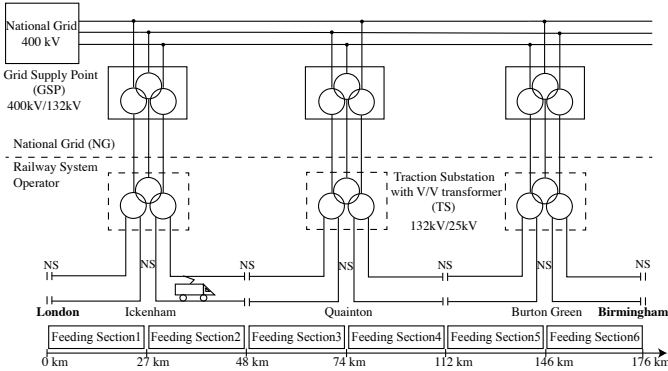

Fig. 6. A conventional connection scheme showing the entire power system connection of the case study.

TABLE III
HS2 PHASE 1: ROUTE AND STATION INFORMATION [31]

Location (km)	Station
0	Euston
9.5	Old Oak Common
156.7	Birmingham Interchange
176	Birmingham Curzon Street

TABLE IV
HS2 PHASE 1: GRID SUPPLY POINTS (GSP), TRACTION SUBSTATIONS AND SECTION INFORMATION [31]

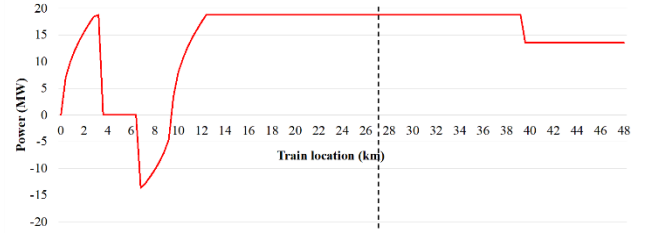| Location (km)	GSP&TS	Neutral Section	Feeding Section
0	-	NS	FS1
27	Ickenham	NS	FS2
48	-	NS	FS3
74	Quainton	NS	FS4
112	-	NS	FS5
146	Burton Green	NS	FS6
176	-	NS	-

Fig. 7. The power profile of a single train travelling through the FS1 (left) and FS2 (right)
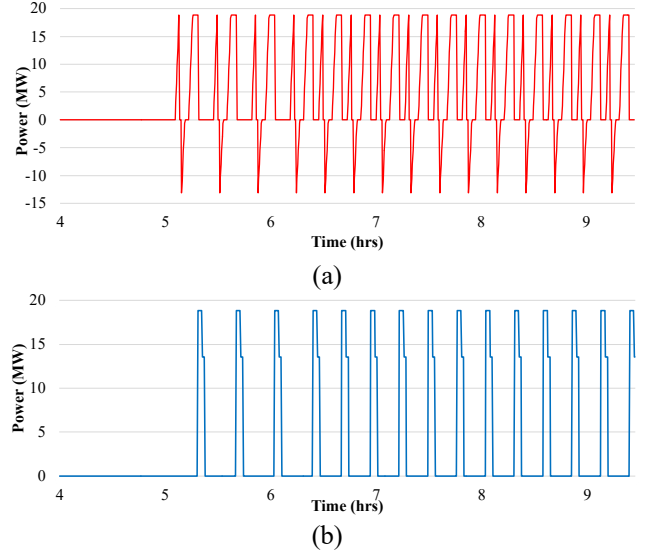

Fig. 8. Multiple-train power profiles from 4 AM to 9 AM in a) FS1 and b) FS2.

Fig. 7 displays an example of the train power profile supplied by the FS1 while traveling from 0 km to 27 km and the FS2 from 27 km to the next neutral section at 48 km. It can be noticed that the RBE is produced during the train travel in FS1, which is the negative power from 6 km to 9 km. On the other hand, the train is in traction mode in FS2. Moreover, the multiple-train power profile of the FS1 and FS2, illustrated in Fig. 8 (a) and Fig. 8 (b), is used for the optimization. It should be noted that reactive power is not considered in this study.

B. Scenarios and parameters

To compare the daily global cost for various combinations of energy sources – grid, ESS, PV farm and wind farm, eight

scenarios are created and summarized in TABLE V. Scenario 1 represents the base scenario where all train demands are supplied by the grid. ESS is installed to capture and reuse the RBE when available in Scenario 2. A solar PV farm is installed to reduce the reliance on grid power in Scenario 3. Then, the addition of ESS is presented in Scenario 4. In Scenario 5, the load demand is supplied by the grid and the wind farm. Similarly, ESS is added in Scenario 6. Next, the grid, PV farm and wind farm are considered in Scenario 7 and lastly, all energy sources are integrated into the system.

TABLE V
SCENARIO DESCRIPTION

Scenarios	Grid	ESS	PV	Wind
1	✓	-	-	-
2	✓	✓	-	-
3	✓	-	✓	-
4	✓	✓	✓	-
5	✓	-	-	✓
6	✓	✓	-	✓
7	✓	-	✓	✓
8	✓	✓	✓	✓

TABLE VI
LOWER LIMITS, UPPER LIMITS AND STEP SIZE FOR VARIABLES

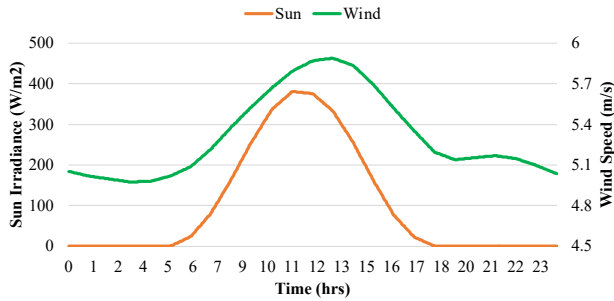| Variable	Lower Limit	Upper limit	Step size
E_{ess}^{rated} (MWh)	0	40	2
$P_{ess}^{rated}(MW)$	0	40	2
$P_{pv}^{rated}(MW)$	0	40	2
$P_{wind}^{rated}(MW)$	0	40	2
$D_{ess1}(km)$	0	27	0.5
$D_{ess2}(km)$	27	48	0.5

Fig. 9. Average sun irradiance and Average wind speed [33]

The lower and upper limits of each variable are tabulated in TABLE VI. The hourly meteorological data for five years from 2015 to 2019 is averaged to reduce uncertainty and computational burden. Then, hourly solar irradiance and wind speed data are interpolated before being applied as input for solar PV and wind farms, as shown in Fig. 9. The solar PV and wind farm parameters are displayed in TABLE VII and TABLE VIII. Additionally, parameters for the energy cost, the carbon cost, the ESS cost and the SFC cost are shown in TABLE IX. In order to ensure that the global optimum is found, a Brute Force (BF) search, which is the algorithm that attempts all conceivable solutions in a problem in order to identify the extrema of the objective function, is adopted. As an exact algorithm, BF guarantees that the best solutions will be found if they exist [32].

TABLE VII
SOLAR PV FARM PARAMETERS

Parameters	Values [29]	Descriptions
$c_{pd,pv}$	50×10^3 £/MW	Pre-development cost
$c_{con,pv}$	400×10^3 £/MW	Construction cost
$c_{om,pv}$	$6700 \cdot T_{pv}$ £/MW	O&M Cost
T_{pv}	35 years	Lifetime of PV farm

TABLE VIII
WIND FARM PARAMETERS

Parameters	Values [29][34]	Descriptions
$c_{pd,wind}$	120×10^3 £/MW	Pre-development cost
$c_{con,wind}$	1000×10^3 £/MW	Construction cost
$c_{om,wind}$	$23500 \cdot T_{wind}$ £/MW	O&M cost
T_{wind}	25 years	Lifetime of Wind farm
v_{ci}	4 m/s	Wind Cut-in speed
v_r	13 m/s	Rated wind speed
v_{co}	23 m/s	Wind Cut-out speed
a	2	Weibull shape parameter
α	0.159	Hellman Height exponent

TABLE IX
PARAMETERS FOR ENERGY COST, SFC COST, CARBON COST, AND ENERGY STORAGE SYSTEM

Parameters	Values [28], [35]	Descriptions
c_{buy}	140 £/MWh	Cost of grid energy
c_{sell}	70 £/MWh	Cost of selling energy to grid
CI	30.8 gCO₂/kWh	Average Carbon intensity
c_{carbon}	18 £/ton	Cost of Carbon emissions
$c_{ess,MWh}$	192 £/MWh	Energy Capacity Cost of ESS
$c_{ess,MW}$	184 £/MW	Power Capacity Cost of ESS
P_{cw}^{rated}	40 MW	Maximum Power Capacity of Contact Wire
r	0.15 Ω/km	Contact wire resistance
SOC_{ess}^{min}	10%	Minimum state of charge
SOC_{ess}^{max}	90%	Maximum state of charge
$T_{tr,fs}$	1/5 and 1/15 hr	Duration in section1 and 2
T_{ess}	10 years	Lifetime of ESS
c_{sfc}	3.46×10^5 £/unit	Cost of SFC per unit
U_{sfc}	2 MVA	Capacity of SFC per unit
T_{sfc}	25 years	Lifetime of SFC

C. Cost analysis

The optimization results for FS1 are displayed in TABLE X. The highest daily cost belongs to Scenario 1 where the load is solely supplied by the grid. Scenario 2 is 200 £/day lower than Scenario 1 with an ESS (2 MWh, 4 MW) installed 10.5 km away from London Euston. The cost is reduced because the RBE is used to supply the upcoming trains. Moreover, with the optimal location of the ESS, the contact wire losses are reduced by around 8 % compared to Scenario 1.

TABLE X
OPTIMIZATION RESULT OF FEEDING SECTION 1

Scenarios	C_{total} (£/day)	E_{cwloss} (MWh/day)	D_{ess} (km)	E_{ess}^{rated} (MWh)	P_{ess}^{rated} (MW)	P_{pv}^{rated} (MW)	P_{wind}^{rated} (MW)
1	15800	6.11	-	-	-	-	-
2	15600	5.64	10.5	2	4	-	-
3	9890	6.46	20	-	-	40	-
4	8870	4.64	15.5	24	10	40	-
5	2540	7.20	20.5	-	-	-	40
6	954	6.25	20	2	10	-	40
7	2540	7.20	20.5	-	-	0	40
8	954	6.25	20	2	10	0	40

TABLE XI
OPTIMIZATION RESULT OF FEEDING SECTION 2

Scenarios	C_{total} (£/day)	E_{cwloss} (MWh/day)	D_{ess} (km)	E_{ess}^{rated} (MWh)	P_{ess}^{rated} (MW)	P_{pv}^{rated} (MW)	P_{wind}^{rated} (MW)
1	10300	3.10	-	-	-	-	-
2	10300	3.10	27	0	0	-	-
3	5330	3.41	30	-	-	40	-
4	4960	2.60	40.5	6	4	40	-
5	-966	3.50	28.5	-	-	-	40
6	-1622	3.57	30.5	2	8	-	40
7	-966	3.50	28.5	-	-	0	40
8	-1622	3.57	30.5	2	8	0	40

With the PV integration in Scenario 3, the optimal size and location of the PV farm are 40 MW and 20 km. The cost dropped to 9890 £/day, which is significant compared to the first and the second scenarios. It is noticed that the contact wire losses slightly go up as the excess power flowed to the grid dissipated as losses. Further cost saving is observed with the integration of the ESS in Scenario 4, where 1020 £/day is saved, and the contact wire loss is the lowest among all scenarios. This results from excess power and RBE are absorbed by the ESS. For this scenario, the installation of a PV farm (40 MW) and an ESS (24 MWh, 10 MW) are required at 15.5 km to achieve the optimal solution.

Without the ESS, the total cost notably decreased by 6330 £/day despite the higher contact wire losses compared to the previous case. To attain this cost saving, a 40 MW wind farm must be connected at 20.5 km. Additionally, the ESS and wind farm are considered in Scenario 6 and the result reveals that by installing the ESS (2 MWh, 10 MW) and a 40 MW wind farm at 20 km, the total cost is remarkably reduced to 954 £/day or approximately 62% reduction and a decline of 0.95 MWh/day of contact wire losses relative to the case without the ESS.

The rated capacities of both PV and wind farms are considered in Scenario 7. However, the result reveals that to minimize the total cost, only a 40 MW wind farm is required to integrate at 20.5 km. This result provides the same outcome as Scenario 5. Considering all variables i.e., the RES location, the energy and power capacity of ESS, and the rated power of PV and wind farms in Scenario 8, the optimization result indicates that installing a 40 MW wind farm and an ESS (2 MWh, 10 MW) at 20 km, is the most economical scheme. It is observed that the result from this scenario is identical to Scenario 6.

TABLE XI presents the results of FS2. The advantages of the RES and ESS are shown, and the same trend is observed. However, because the train travelling in this section is in traction mode, the ESS is not essential in Scenario 2; hence, the

cost and losses in Scenarios 1 and 2 are identical. The main difference is that instead of purchasing, the railway operator can sell the power, which can be seen as a negative cost in Scenarios 5 to 8.
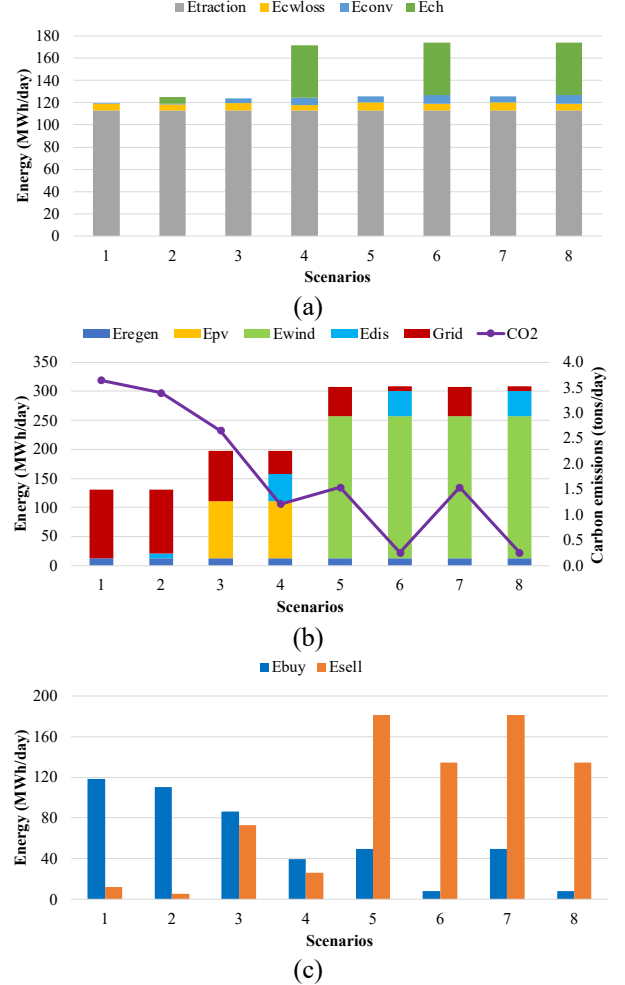

(a)

(b)

(c)

Fig. 10. Energy flow charts of FS1 a) energy demand b) energy supply and c) exchange energy with the grid.

D. Energy flow analysis

The energy demand in FS1 is broken down according to loads, depicted in Fig. 10 (a), where the traction load accounts for approximately 95% or 112.8 MWh/day in the scenarios without the ESS. Conversion loss (E_{conv}) exists only when the conversion devices are operated, and it is proportional to the amount of power generated by RES and the charging and discharging power of the ESS. The green bars represent the energy charged (E_{ch}) into the ESS. With RES, the ESS is charged with a large amount of excess energy.

The breakdown of the energy supply is illustrated in Fig. 10 (b). In the scenarios without RES, the demand is met by the power purchased from the grid. However, there is a small amount of energy sold to the grid, as seen in Scenarios 1 and 2 in Fig. 10 (c), which is the unused RBE. Despite having the ESS in Scenario 2, there is a small amount of RBE that is not captured since the ESS reached the upper limit capacity. With RES integration, the required power from the grid falls considerably. In Scenarios 4 and 5, the PV farm produced 98.6 MWh/day.

Furthermore, from Scenarios 5 to 8, the energy from the wind farm dominates the grid power, causing a large amount of excess power sold to the grid. As seen in Fig. 10 (c), the energy sold to the grid is greater than the energy purchased from the grid. Additionally, the carbon emissions significantly declined in cases with the RES and ESS. Scenarios 4, 6 and 8 depict the benefits of the ESS in reducing the required power from the grid, hence lowering carbon emissions. It is worth mentioning that the attribute of energy flow of FS2 is similar to FS1.
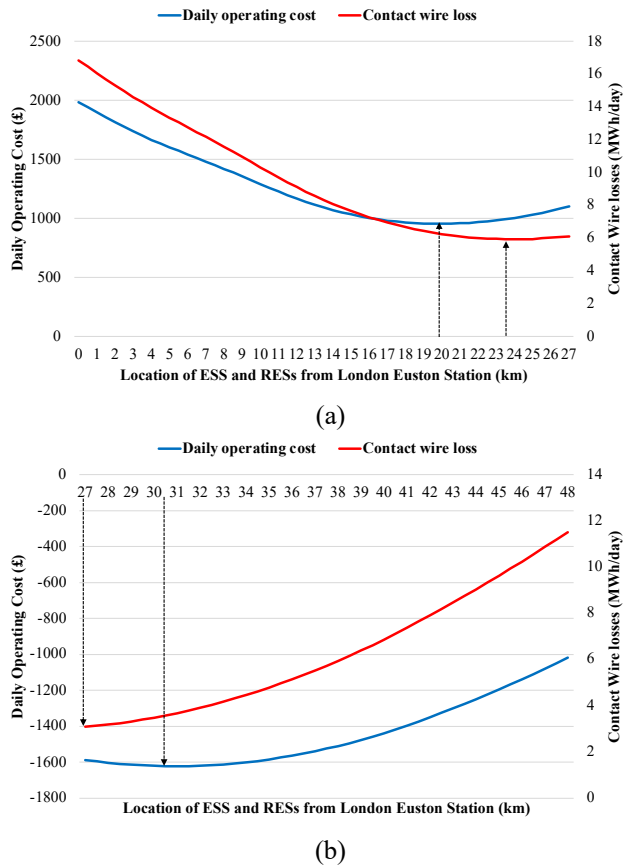

(a)

(b)

Fig. 11. Total daily cost and contact wire losses with different RES and ESS locations a) feeding section 1, based on a 2 MWh, 10 MW ESS and a 40 MW wind farm b) feeding section 2, based on a 2 MWh, 8 MW ESS and a 40 MW wind farm.

Fig. 11 illustrates the total daily cost and the contact wire losses for different ESS and RES locations in feeding sections 1 and 2. It can be seen that the location with the minimum total cost is different from the location with the minimum contact wire loss. For instance, in Fig. 11 (a), the lowest contact wire loss is found where the ESS and wind farm in feeding section 1 are installed at 23.5 km. Nevertheless, the total cost in this location is higher than installing at 20 km, which is the optimal location. The contact wire losses can be separated into two parts: loss due to the flow of current to trains and loss due to the flow of current to the grid (excess power from renewables). Hence, more energy is needed to compensate for the loss when the current is supplied to trains, and less energy is fed to the grid after subtracting the loss. The results reveal that the locations where the minimum contact wire losses are found tend to be near or at the traction substation. This is because a major

proportion of contact wire losses is generated by excess energy flow to the grid from the wind farm. Thus, if the renewables are installed close to the traction substation, the reduction of contact wire losses will be observed. Nonetheless, this increases another part of contact wire losses (current flow to trains) and slightly increases demand. The railway system operator will need to buy more energy if the power from wind farm and energy storage are insufficient. Therefore, the total cost is rising, which is the reason why the lowest contact wire loss location is not at the same spot as the lowest total cost.

VI. CONCLUSION

This paper proposed the integration scheme for renewable energy sources and energy storage systems into the AC railway power supply system. Additionally, a comprehensive model with an energy management system is developed to reduce the daily global cost. Finally, the Brute Force method is employed to optimize the best integrating location, ESS power and energy capacity, including the sizing of PV and wind farms, to achieve minimum total daily cost.

The result from the case study shows that energy storage played a crucial role in storing the regenerative braking energy and excess energy from renewable energy sources. From the case study, around 1.3% of the global cost could be saved if the ESS is installed to capture the regenerative energy. Another 10% and 58% saved by absorbing the excess energy from the PV and wind farm, compared to the same scenarios without the ESS. With the optimal location, the contact wire losses are considerably reduced in the scenarios with the ESS. The PV and wind farms are the main contributor to reducing the reliance on grid energy and carbon emissions. However, it has been found that integrating a wind farm is a better way to reduce and/or gain money and reduce carbon emissions compared to a PV farm. It should be noted that the solar irradiance and wind speed data used in this study are based on the UK location. Therefore, the result may differ in a different location.

REFERENCES

[1] C. o. C. Change, "Net Zero: The UK's contribution to stopping global warming," Committee on Climate ChangeMay 2019 2019.
[2] B. An, Y. Li, J. M. Guerrero, W.-J. Lee, L. Luo, and Z. Zhang, "Renewable Energy Integration in Intelligent Railway of China: Configurations, Applications and Issues," IEEE Intelligent Transportation Systems Magazine, pp. 2-22, 2020.
[3] M. Brenna, F. Foiadelli, and H. J. Kaleybar, "The Evolution of Railway Power Supply Systems Toward Smart Microgrids: The concept of the energy hub and integration of distributed energy resources," IEEE Electrification Magazine, vol. 8, no. 1, pp. 12-23, 2020.
[4] S. Tang, X. Huang, Q. Li, N. Yang, Q. Liao, and K. Sun, "Optimal Sizing and Energy Management of Hybrid Energy Storage System for High-Speed Railway Traction Substation," Journal of Electrical Engineering & Technology, vol. 16, no. 3, pp. 1743-1754, 2021/05/01 2021.
[5] W. Deng, C. Dai, W. Chen, and S. Gao, "Experimental Investigation and Adaptability Analysis of Hybrid Traction Power Supply System Integrated With Photovoltaic Sources in AC-Fed Railways," IEEE Transactions on Transportation Electrification, vol. 7, no. 3, pp. 1750-1764, 2021.
[6] S. Boudoudouh and M. Maaroufi, "Renewable Energy Sources Integration and Control in Railway Microgrid," IEEE Transactions on Industry Applications, vol. 55, no. 2, pp. 2045-2052, 2019.
[7] H. Novak, V. Lesic, and M. Vasak, "Hierarchical Model Predictive Control for Coordinated Electric Railway Traction System Energy Management," IEEE Transactions on Intelligent Transportation Systems, vol. 20, no. 7, pp. 2715-2727, 2019.

[8] L. Razik, N. Berr, S. Khayyam, F. Ponci, and A. Monti, "REM-S–Railway Energy Management in Real Rail Operation," IEEE Transactions on Vehicular Technology, vol. 68, no. 2, pp. 1266-1277, 2019.

[9] Z. Tian, P. Weston, N. Zhao, S. Hillmansen, C. Roberts, and L. Chen, "System energy optimisation strategies for metros with regeneration," Transportation Research Part C: Emerging Technologies, vol. 75, pp. 120-135, 2017/02/01/ 2017.

[10] C. Feng, Z. Gao, Y. Sun, and P. Chen, "Electric railway smart microgrid system with integration of multiple energy systems and power-quality improvement," Electric Power Systems Research, vol. 199, p. 107459, 2021/10/01/ 2021.

[11] Y. Ying, Q. Liu, M. Wu, and Y. Zhai, "The Flexible Smart Traction Power Supply System and Its Hierarchical Energy Management Strategy," IEEE Access, vol. 9, pp. 64127-64141, 2021.

[12] S. D'Arco, L. Piegari, and P. Tricoli, "Comparative Analysis of Topologies to Integrate Photovoltaic Sources in the Feeder Stations of AC Railways," IEEE Transactions on Transportation Electrification, vol. 4, no. 4, pp. 951-960, 2018.

[13] Y. Liu, M. Chen, Z. Cheng, Y. Chen, and Q. Li, "Robust Energy Management of High-Speed Railway Co-Phase Traction Substation With Uncertain PV Generation and Traction Load," IEEE Transactions on Intelligent Transportation Systems, vol. 23, no. 6, pp. 5079-5091, 2022.

[14] J. A. Aguado, A. J. S. Racero, and S. d. l. Torre, "Optimal Operation of Electric Railways With Renewable Energy and Electric Storage Systems," IEEE Transactions on Smart Grid, vol. 9, no. 2, pp. 993-1001, 2018.

[15] S. R. Salkuti, "Optimal Operation of Electrified Railways with Renewable Sources and Storage," Journal of Electrical Engineering & Technology, vol. 16, no. 1, pp. 239-248, 2021/01/01 2021.

[16] S. Park and S. R. Salkuti, "Optimal Energy Management of Railroad Electrical Systems with Renewable Energy and Energy Storage Systems," Sustainability, vol. 11, no. 22, 2019.

[17] I. Sengor, H. C. Kilickiran, H. Akdemir, B. Kekezoglu, O. Erdinc, and J. P. S. Catalao, "Energy Management of a Smart Railway Station Considering Regenerative Braking and Stochastic Behaviour of ESS and PV Generation," IEEE Transactions on Sustainable Energy, vol. 9, no. 3, pp. 1041-1050, 2018.

[18] M. Chen, Z. Liang, Z. Cheng, J. Zhao, and Z. Tian, "Optimal Scheduling of FTPSS With PV and HESS Considering the Online Degradation of Battery Capacity," IEEE Transactions on Transportation Electrification, vol. 8, no. 1, pp. 936-947, 2022.

[19] '24-hour Simulation of a Vehicle-to-Grid (V2G) System', https://uk.mathworks.com/help/physmod/sps/ug/24-hour-simulation-of-a-vehicle-to-grid-v2g-system.html, accessed 4 June 2022.

[20] VESTAS, "General Specification: V90-1.8/2.0 MW 50 Hz VCS", 2010, p. 16.

[21] G.B. Gharehpetian, and S.M. Mousavi, "Distributed generation systems", Butterworth-Heinemann, Oxford, United Kingdom, 2017, p. 31.

[22] G. L. Johnson, "Wind energy systems," Proc. IEEE, vol. 105, no. 11, pp. 2116–2131, 2017.

[23] C. Demoulias, "A new simple analytical method for calculating the optimum inverter size in grid-connected PV plants," *Electr. Power Syst. Res.*, vol. 80, no. 10, pp. 1197–1204, 2010.

[24] G.B. Gharehpetian, and S.M. Mousavi, "Energy storage systems," in *Distributed generation systems*, Butterworth-Heinemann, Oxford, United Kingdom, 2017, ch.7, pp.336-337.

[25] ABB, "ABB solar inverters: Explore the industry's broadest portfolio", 2016, pp.66.

[26] S. Hadi, "Power System Analysis," 1st ed., McGraw-Hill, New York, 1999, pp. 70–135.

[27] ABB, "More Power for Railway Lines: Dynamic Shunt Compensation and Static Frequency Conversion for 50 Hertz (Hz) Traction Power Supply", 2016.

[28] Cole, Wesley, A. Will Frazier, and Chad Augustine, "Cost Projections for Utility- Scale Battery Storage: 2021 Update," Golden, CO: National Renewable Energy Laboratory. NREL/TP-6A20-79236. Available: https://www.nrel.gov/docs/fy21osti/79236.pdf.

[29] Department for Business, Energy & Industrial Strategy, "Electricity Generation Costs 2020", Aug 2020, pp. 10.

[30] F. Kiessling, R. Puschmann, A. Schmieder, and E. Schneider, "Contact Lines for Electric Railways," 2018, pp. 425-455 .

[31] UK Government, "HS2 Phase One Plan and Profile Maps: London to the West Midlands." Available:

https://www.gov.uk/government/collections/hs2-plan-and-profile-maps-between-london-and-the-west-midlands.

[32] Z. Tian, "System Energy Optimisation Strategies for DC Railway Traction Power Networks," Ph.D. Thesis, Dept. Elect. Eng., Univ. Birmingham, United Kingdom, 2014. [online]. Available: https://etheses.bham.ac.uk/

[33] S. Pfenninger and I. Staffell, "Long-term patterns of European PV output using 30 years of validated hourly reanalysis and satellite data," Energy, vol. 114, pp. 1251–1265. DOI: 10.1016/j.energy.2016.08.060.

[34] VESTAS, "2 MW platform: V90-2.0 MW IEC IIA/IEC S Facts & figures", 2020, p. 9.

[35] National Grid, "Electricity Ten Year Statement 2014 (Appendix E23 Unit costs)," p. 69.

Nakaret Kano (Student member, IEEE) received the B.Eng degree in electrical engineering from King's Mongkut Institute of Technology Ladkrabang, Bangkok, Thailand in 2010. He received the M.Eng degree in geosystem exploration and petroleum geoengineering from Asian Institute of Technology, Pathumthani, Thailand in 2014. He is currently pursuing a PhD degree in electrical and electronic engineering at the University of Birmingham. His main research interests include railway power supply system, renewable generations, energy storages and energy management system in traction power networks.

Zhongbei Tian received the B.Eng in Huazhong University of Science and Technology, Wuhan, China, in 2013. He received the B.Eng. and PhD degree in Electrical and Electronic Engineering from the University of Birmingham, Birmingham, U.K., in 2013 and 2017. He is currently a Lecturer in Electrical Energy Systems at the University of Liverpool. His research interests include railway traction power system modelling and analysis, energy-efficient train control, energy system optimisation, and sustainable transport energy systems integration and management.

Nutthaka Chinomi received the BEng degree in Electrical Engineering from the King Mongkut's Institute of Technology Ladkrabang, Bangkok, Thailand, in 2015. She received the MSc degree in Railway Systems Engineering and Integration from the University of Birmingham, Birmingham, UK, in 2020. She is currently pursuing her PhD in the Department of Electrical Engineering and Electronics at the University of Liverpool, Liverpool, UK. Her research interests include railway system modelling, renewable energy integration, and energy system optimisation

Xiaoguang Wei received the Ph.D. degree in electrical engineering from Southwest Jiaotong University, Chengdu, China, in 2019, where he is currently an Assistant Professor with the School of Electrical Engineering. His research interests include power market and energy system security.

Stuart Hillmansen received his Ph.D. degree from Imperial College, London. He is currently a Professor in Railway Traction Systems with the Department of Electronic, Electrical, and Systems Engineering at the University of Birmingham. He is a member of the Birmingham Centre for Railway Research and Education where he leads the Railway Traction Research Group, whose portfolio of activities is supported by the railway industry and government. His research interests include hybrid traction systems for use in railway vehicles and the modeling and measurement of energy consumption for railway systems.